molecules

MDPI

Article

Molecular Modeling of Epithiospecifier and Nitrile-Specifier Proteins of Broccoli and Their Interaction with Aglycones

Juan Román [1], Dorian González [1], Mario Inostroza-Ponta [2] and Andrea Mahn [1,*]

[1] Departamento de Ingeniería Química, Universidad de Santiago de Chile, Avenida Libertador Bernardo O'Higgins 3363, Estación Central, Santiago 9170019, Chile; juan.romana@usach.cl (J.R.); dorian.gonzalez@usach.cl (D.G.)

[2] Departamento de Ingeniería Informática, Universidad de Santiago de Chile, Avenida Libertador Bernardo O'Higgins 3363, Estación Central, Santiago 9170019, Chile; mario.inostroza@usach.cl

* Correspondence: andrea.mahn@usach.cl; Tel.: +56-2-2718-1833

Received: 23 December 2019; Accepted: 3 February 2020; Published: 11 February 2020

Abstract: Glucosinolates are secondary plant metabolites of *Brassicaceae*. They exert their effect after enzymatic hydrolysis to yield aglycones, which become nitriles and epithionitriles through the action of epithiospecifier (ESP) and nitrile-specifier proteins (NSP). The mechanism of action of broccoli ESP and NSP is poorly understood mainly because ESP and NSP structures have not been completely characterized and because aglycones are unstable, thus hindering experimental measurements. The aim of this work was to investigate the interaction of broccoli ESP and NSP with the aglycones derived from broccoli glucosinolates using molecular simulations. The three-dimensional structure of broccoli ESP was built based on its amino-acid sequence, and the NSP structure was constructed based on a consensus amino-acid sequence. The models obtained using Iterative Threading ASSEmbly Refinement (I-TASSER) were refined with the OPLS-AA/L all atom force field of GROMACS 5.0.7 and were validated by Veryfy3D and ERRAT. The structures were selected based on molecular dynamics simulations. Interactions between the proteins and aglycones were simulated with Autodock Vina at different pH. It was concluded that pH determines the stability of the complexes and that the aglycone derived from glucoraphanin has the highest affinity to both ESP and NSP. This agrees with the fact that glucoraphanin is the most abundant glucosinolate in broccoli florets.

Keywords: broccoli; epithiospecifier protein; nitrile-specifier protein; aglycones; molecular docking

1. Introduction

Glucosinolates (GLS) constitute a large group of non-volatile, nitrogen- and sulfur-containing secondary metabolites mainly found in *Brassicaceae* family [1,2]. Their chemical structure consists of a β-d-glucopyranose residue linked to a thiohydroximate-O-sulfonate group by sulfur bridge, and an alkyl, aralkyl, or indolyl side chain (R) [3,4].

GLS play important roles in plant defense against biotic stress [7]. GLSs are stored in vacuoles or in specialized S-cells [8,9], and are relatively stable in the intact plant. However upon cell disruption, either by the action of microorganisms, insects or herbivores, GLS are broken down resulting into different compounds, such as isothiocyanates (ITC), thiocyanates (TCN), nitriles (NIT), or epithionitriles (EPT) (Figure 1), depending on the chemical conditions [10–12]. The reaction proceeds through a two-step mechanism. First, GLSs are hydrolyzed by myrosinase to yield an unstable aglycone intermediate (thiohydroximate-O-sulfonate). Second, the aglycone turns into isothiocyanates, thiocyanates, epithionitriles or nitriles, depending on pH, cofactors and specifier proteins [13].

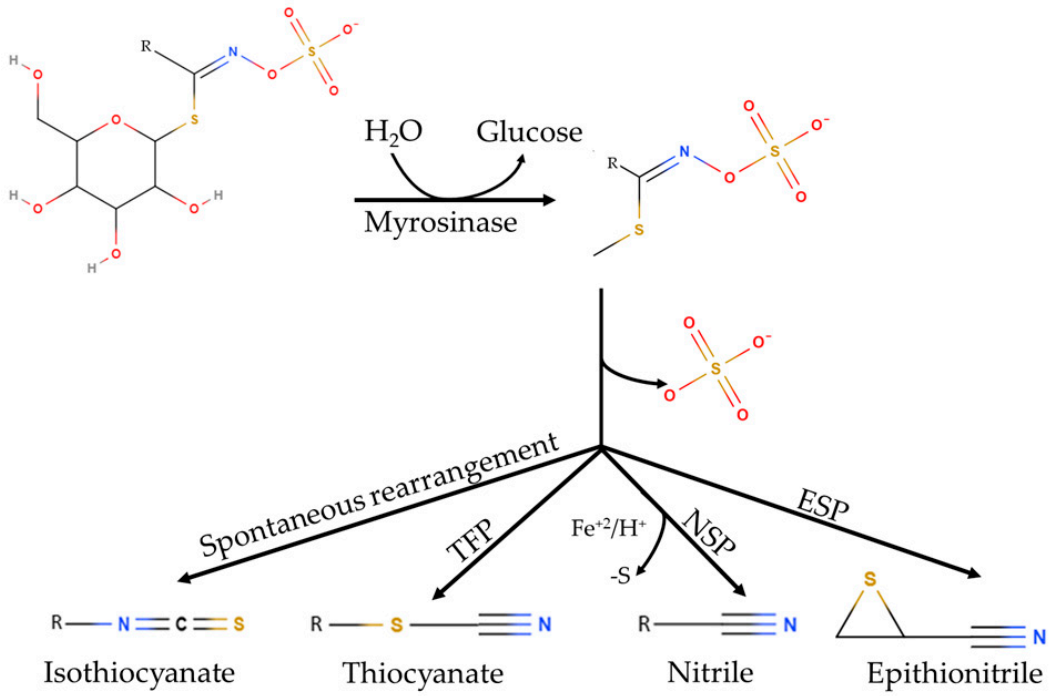

Figure 1. Glucosinolate hydrolysis. Glucosinolates are hydrolyzed by myrosinase yielding unstable aglycones. These aglycones can form isothiocyanates spontaneously, or other hydrolysis products, depending on the presence of specifier proteins (thiocyanate-forming proteins (TFP), epithiospecifier (ESP), nitrile-specifier proteins (NSP)) modified from [5,6].

Specifier proteins act on aglycones stabilizing them into compounds with antimicrobial, insecticide, and nematicide activity, showing no hydrolytic activity on glucosinolates themselves [14,15]. The formation mechanism of these products has not been elucidated so far. Some authors point out that specifier proteins are enzymes that act on aglycones [13,16]. Nevertheless, this has not been validated through kinetic studies or aglycone-protein crystallization studies mainly because of aglycones instability [15]. Specifier proteins may have a role in balancing the defense system of plants against generalist versus specialist herbivores, through different hydrolysis products [10,17]. Specifier proteins are grouped according to the final reaction product. Thiocyanate-forming proteins (TFP) promote the formation thiocyanates, and occur in few plant species (*Coronopus didymus*, *Eruca sativa*, *Lepidium ruderale*, *Lepidium sativum*, and *Thlaspi arvense*) [15,18,19]. Thiocyanates formation occurs only from allyl-GLS, 4-methylthiobutyl-GLS and benzyl-GLS [15,20,21]. Nitrile-specifier proteins (NSP) promote simple nitrile formation [22–24]. Epithiospecifier proteins (ESP) are relatively labile and promote epithionitriles formation [14]. ESP has a molecular weight between 30 and 40 kDa and is stabilized by Fe^{2+}. Epithionitriles formation requires the presence of a terminal double bond in the glucosinolate aglycone [15,22]. Some studies revealed that ESP also promotes the formation of simple nitriles from aglycones lacking a terminal double bond [6,13].

Epithiospecifier protein (ESP) was isolated from *Crambe abyssinica* for the first time in 1973 and named for promoting epithionitriles formation [14]. In later studies, ESP was purified from *Brassica napus* L. [16,25]. To date, only one study on broccoli ESP has been reported. In that study, the formation of sulforaphane or sulforaphane nitrile were investigated by measuring ESP activity isolated from broccoli cv. Packman. Also, broccoli ESP was cloned and expressed in *Escherichia coli* obtaining 43 kDa recombinant protein [6,13]. To date, only *A. Thaliana* ESP structure has been resolved by X-ray diffraction (PDB code 5GQ0) [26].

Nitrile-specifier proteins (NSP) has been poorly studied so far. One of the first studies was carried out with *Pieris rapae* (white cabbage, *Lepidoptera*: *Pieridae*) NSP [27]. Five nitrile-specifier proteins (AtNSP1 to AtNSP5) in *A. thaliana* were identified later [22,23,28]. Currently, there is only one structure

for NSP1 from *Arabidopsis thaliana* resolved by X-ray diffraction [29]. No studies about molecular interaction between broccoli ESP and broccoli NSP with aglycones are available so far.

In broccoli (*Brassica oleracea* var. *italica*), the main glucosinolate is glucoraphanin (GFN), and its hydrolysis at neutral pH yields preferably sulforaphane (SFN) which is one of the most potent food-derived anticancer compounds and also exhibits antimicrobial activity [30]. These facts encouraged the study of the myrosinase-glucosinolate system in broccoli in recent years. Different strategies have been proposed to increase SFN content in processed broccoli minimizing the formation of competing compounds such as nitriles and epithionitriles, which offer no health beneficial effects to the consumer. The strategies include blanching [31], high-pressure treatment [32], and microwave processing [33]. However, the complete conversion of GFN into SFN has not been achieved so far. Knowing the mechanism of action of broccoli ESP and NSP on aglycones occurring in broccoli would help in designing better strategies to maximize the conversion of glucosinolates into health-promoting compounds. The high instability of aglycones hinders experimental measurements. Hence, in this work, we studied the interaction between broccoli ESP and NSP with aglycones occurring in broccoli through molecular simulation tools.

2. Results and Discussion

2.1. Identification of the Main Glucosinolates Found in Broccoli Inflorescences

In order to select the aglycones to perform the molecular simulations, the main glucosinolates present in broccoli inflorescences were identified. Figure 2A shows the chromatogram of glucosinolates found in broccoli inflorescences. Five peaks were identified, according to Table 1. Figure 2B presents the mass spectrum of peak 3, corresponding to glucoraphanin. Figure 2C shows the structures of the identified glucosinolates.

Table 1. Identification of glucosinolates detected in broccoli inflorescences. t_R is the retention time and $[M\text{-}H]^-$ is the m/z signal.

Peak	Glucosinolate	t_R (min)	$[M\text{-}H]^-$	MS^2 (m/z)	References
GI	Glucoiberin	3.8	422.3	357.8; 258.6; 274.6; 226.3; 197.1	[34–36]
SIN	Sinigrin	4.7	358.4	258.6; 161.3; 194.3; 274.4; 242.6	[35–37]
GRA	Glucoraphanin	6.1	436.4	371.9; 420.7; 258.7; 177.3; 290.7; 193.5	[34–38]
HGBS	Hydroxy-glucobrassicin	12.4	463.3	364.7; 266.7; 284.7; 159.3; 239.7; 259.3	[36,38]
GBS	Glucobrassicin	15.8	447.5	258.7; 274.7; 241.0; 205.0; 290.7; 260.7	[34,36,39]

The MS/MS product ions obtained from the M− anions (Table 1; Figure 2B and Figure S1) revealed two groups of typical fragments: one associated with the common moiety of the glucosinolates and the other providing diagnostic ions for the identification of the variable side chain. Some fragmentations differed from those described in literature. The m/z 436.4 signal observed at peak 3 (t_R 6.1 min) fragmented mainly to m/z 371.9 (Figure 2B) due to the loss of the methyl sulfoxide moiety; this peak was identified as glucoraphanin. The intensity distribution of fragments from glucobrassicin and hydroxy-glucobrassicin differed from those described in the literature, probably because of the different instruments used and the different fragmentation energies used. In this study, 2-propenyl glucosinolate (2PROP-GLS) and 3-(methylsulfinyl)propyl glucosinolate (3MSOP-GLS) were also identified (Table 1). Leng et al. [40] identified seven glucosinolates (GLS) in broccoli sprouts, with glucoraphanin being the most abundant. Wang et al. [41] reported seven aliphatic GLS in broccoli seeds, with glucoraphanin being the most abundant. Other authors reported that the main GLS in broccoli is glucoraphanin, followed by hydroxyl-glucobrassicin [4,42,43]. Accordingly, the five GSL detected in broccoli florets agree with the results found in the literature.

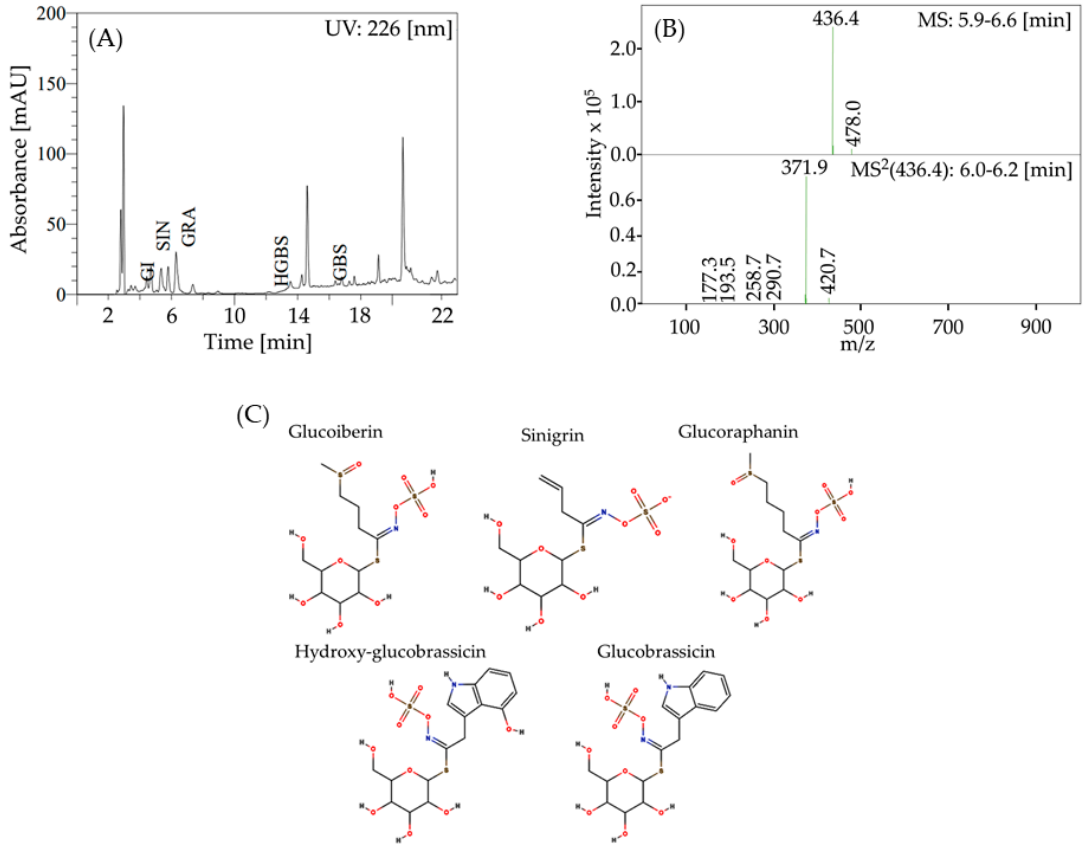

Figure 2. (**A**) High Performance Liquid Chromatography with Photo Diode Array (HPLC-PDA) chromatogram of glucosinolate profile of broccoli inflorescences. Detection at 226 nm. Peaks: (GI) glucoiberin, (SIN) sinigrin, (GRA) glucoraphanin, (HGBS) hydroxy-glucobrassicin, and (GBS) glucobrassicin. (**B**) Liquid Chromatography—Mass Spectrometry (LC-MS) spectra of glucoraphanin. (**C**) Structures of the major glucosinolates identified in broccoli. Figure S1 shows the mass spectra of glucoiberin, sinigrin, hydroxy-glucobrassicin, and glucobrassicin.

2.2. Homology Modeling

The amino acid sequence of broccoli nitrile-specifier proteins (NSP) has not been reported to date. Therefore, a multiple alignment was performed using Clustal W 2.0.12 including sequences of homolog organisms, in order to build a consensus sequence. The homologous NSP sequences were obtained from *Arabidopsis thaliana* (Q9SDM9), *Brassica rapa* subsp. *pekinensis* (M4FIJ4), *Brassica napus* (A0A078G479), and *Brassica oleracea* var. *oleracea* (A0A0D3AD54) (Figure 3).

The consensus amino acid sequence of NSP consisted of 467 residues (Table S1), which encode for a protein with an estimated molecular mass of 51.1 kDa and a pI of 5.8. The amino acid sequence of broccoli epithiospecifier (ESP) was retrieved from the UniProtKB database (UniProtKB code: Q4TU02), and it consists of 343 amino acid residues, with an estimated molecular mass of 37.7 kDa and pI of 5.3. Simple alignment between *A. thaliana* and broccoli sequences gave identities of 80% for NSP and 76% for ESP. Since identities of 80% or lower usually imply structural differences, in this work structural models for broccoli ESP and NSP were built.

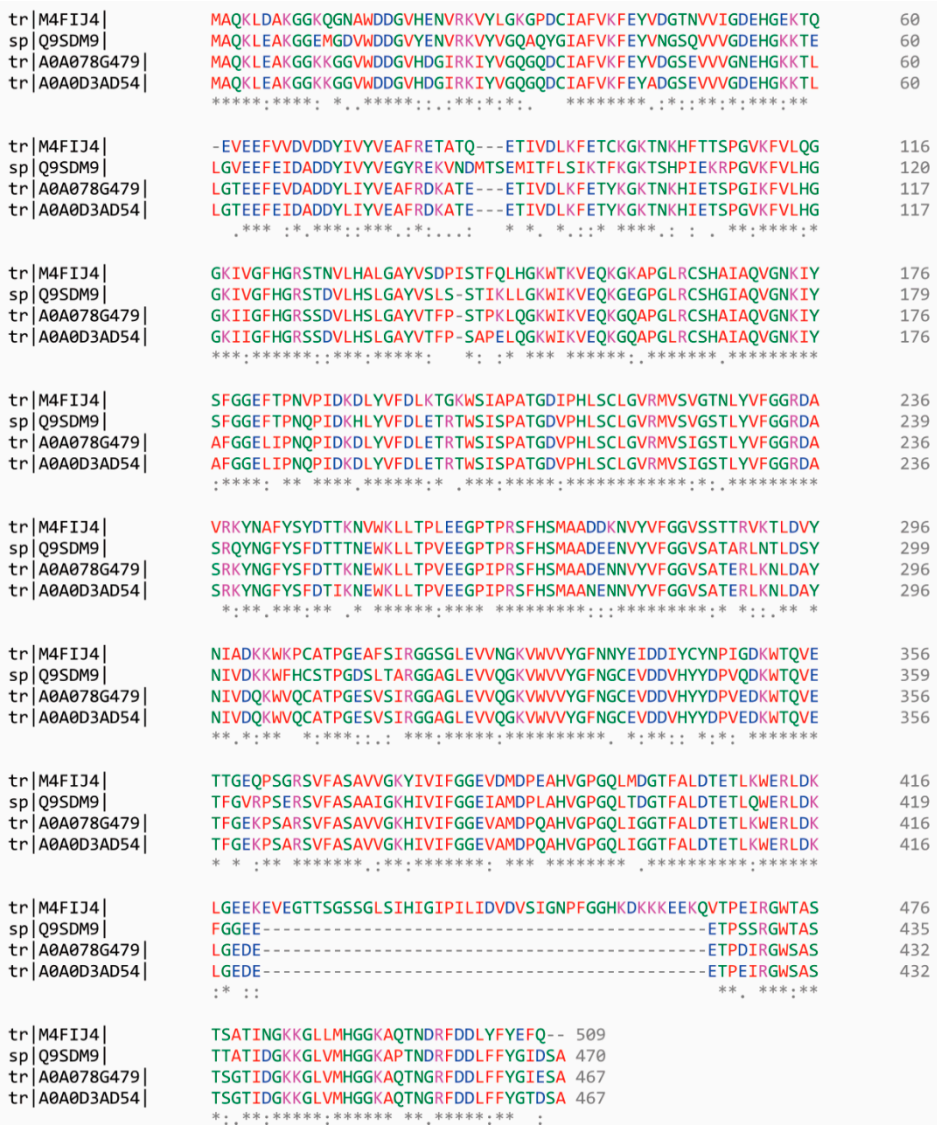

Figure 3. Multiple alignments of Nitrile-specifier Protein (NSP) from broccoli homolog organisms (Q9SDM9, M4FIJ4, A0A078G479, and A0A0D3AD54), generated by means of Clustal W. Gaps and conservation residues were denoted in dashes (-) and asterisks (*), respectively. In addition, colon (:) and period (.) indicate strong and weak properties conservation between groups, respectively. The color code represents the physicochemical property of the amino acid (red: small or hydrophobic, blue: acidic; magenta: basic; green: hydroxyl or sulfhydryl or amine; grey: unusual amino/imino acids).

2.3. Modeling and Refinement of NSP and ESP Structures

The three-dimensional structural models of nitrile-specifier proteins (NSP) and epithiospecifier (ESP) were built using the Iterative Threading ASSEmbly Refinement (I-TASSER) server 5.1 based on the consensus sequence derived for NSP and in the reported sequence of ESP (Q4TU02). Among the five models proposed by I-TASSER for each protein, those showing the highest C-score and TM-score higher than 0.5 were chosen. For the NSP model the C-score was 1.87, and TM- score was 0.98. For the ESP model, the C-score was 1.40, and the TM-score was 0.91. The NSP model (Figure 4A), showed an "all-β" topology with 40 β-sheets and 43 loops. The ESP model (Figure 4B), showed a β - barrel topology, with 29 β-sheets and 29 loops.

The stability and dynamic properties of ESP and NSP models were evaluated using molecular dynamics (MD) simulations. To identify the energetically stable conformations, MD simulation was observed up to 60 ns. The root-mean-square deviation (RMSD) values were examined during the

60 ns of simulation in order to check the structural stability of models. RMSD values of ESP and NSP backbone atoms reached the equilibrium state after 25 ns for both proteins. The average RMSD obtained for ESP was 0.30 (nm) after 25 ns, and remained stable throughout the course of the simulation (Figure 5A). The average RMSD of NSP was 0.25 (nm), and it remained stable after 50 ns simulation (Figure 5B).

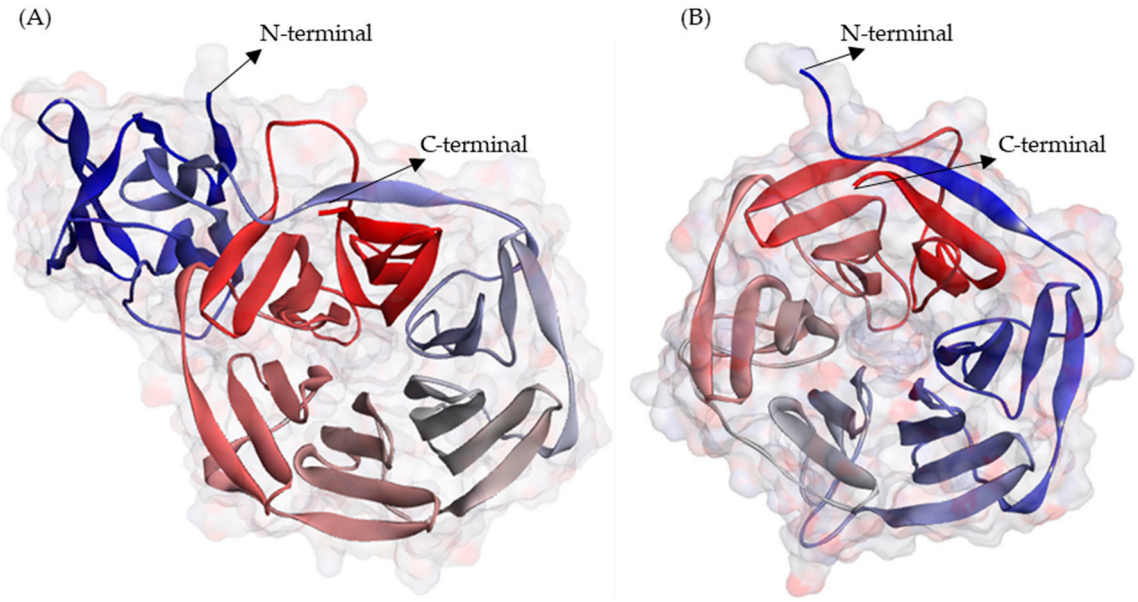

Figure 4. Three-dimensional structure models of (**A**) Nitrile-specifier Protein (NSP) and (**B**) Epithiospecifier Protein (ESP) from broccoli. The models were represented using DS 3.5 visualizer, and colors of N-to-C terminal are based on their secondary structure. The models are available at PMDB (https://bioinformatics.cineca.it/PMDB/) with the identifier PM0082618 for NSP and PM0082617 for ESP.

The ESP and NSP models were validated by ERRAT and Verify3D tools. According to the analysis of error values for each residue made by ERRAT, the average overall quality factor for ESP and NSP models were 85.4% and 82.1%, respectively, which is considered reliable [44]. Additionally, according to Verify3D evaluation, 99% of the ESP residues and 94.4% of the NSP residues had a 3D-score higher than 0.2, which indicates residues are in stable positions. Accordingly, the structural models were accepted as valid [45]. The results of the validation (Figures S2 and S3) confirm that the model quality was satisfactory. The number of H-bonds in the structural models of ESP and NSP was determined during the molecular dynamic's simulations, and are presented in Figure S4. In ESP, H-bonds number fluctuates between 200 and 230, while in NSP varied from 300 to 320, along with the 60 ns simulations. H-bonds number of ESP was lower than NSP because ESP is 124 residues shorter. The results suggest that H-bonds do not vary significantly along the 60 ns trajectory. NSP and ESP models were deposited in the Protein Model DataBase (PMDB) with the access code PM0082618 and PM0082617, respectively (https://bioinformatics.cineca.it/PMDB/). These models were used for molecular docking simulations.

2.4. Molecular Interaction of NSP and ESP with Aglycones

The molecular docking simulations were carried out at different pH (1.0, 3.0, 5.0, 7.0), based on the pH range reported for epithiospecifier (ESP) and nitrile-specifier protein (NSP) [16,21–24,28,30,31]. The five aglycones considered in this study (3MSOP, 2PROP, 4MSOB, 4OHI3M, and I3M, see Table 2) were chosen based on the precursor glucosinolates detected in broccoli inflorescences. Binding sites identification was made with the SiteMap tool of Schrödinger suite 1–2019 [46,47]. SiteMap scores above 1.000 are generally considered as possible binding sites [48]. ESP SiteMap score for the selected site was 1.092, and that for NSP was 1.106. Despite using structural models that are less reliable than

crystallographic structures, conservation of the residues that belong to the substrate binding sites could be observed when comparing with ESP and NSP from *A. thaliana*.

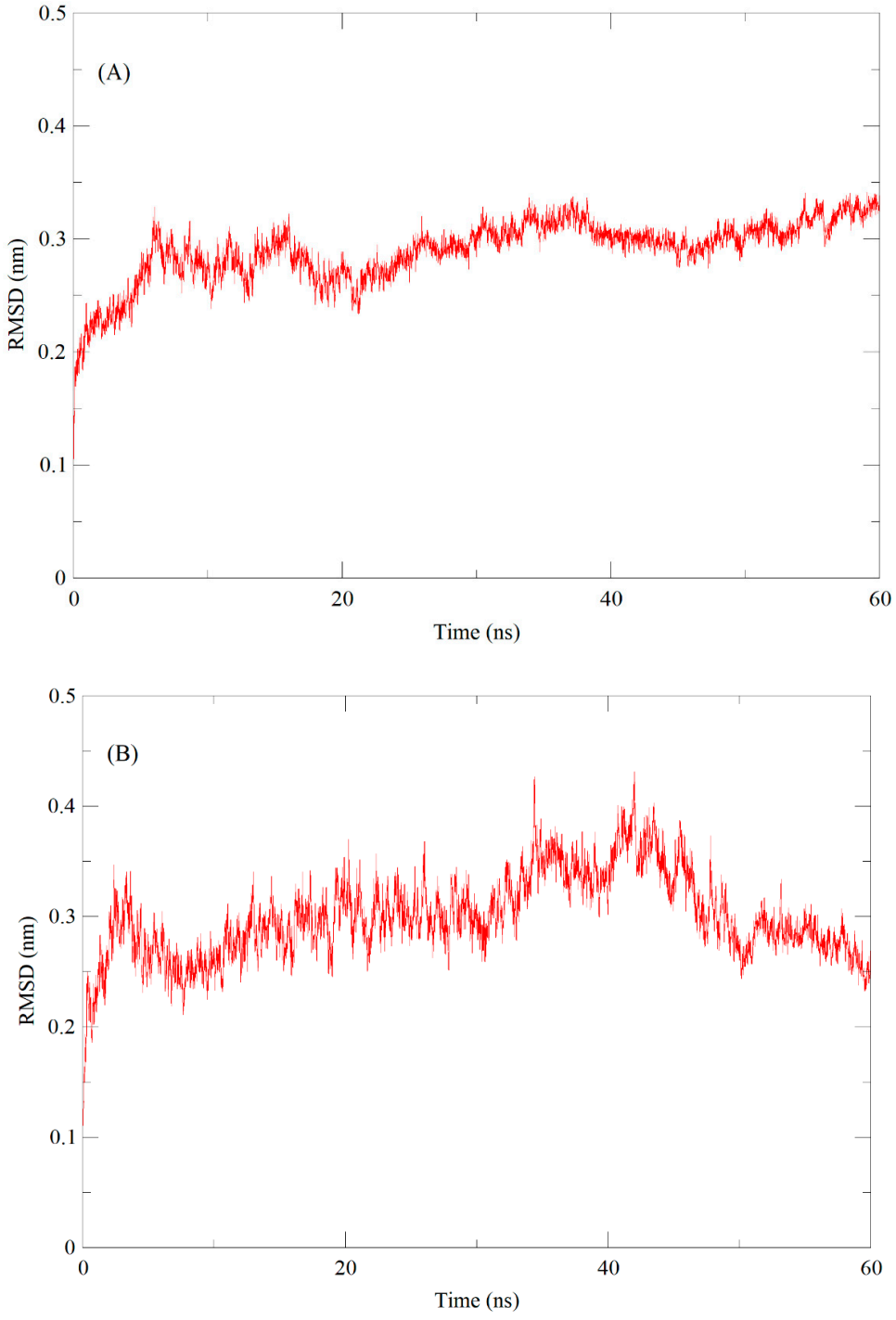

Figure 5. Molecular dynamics-based Epithiospecifier Protein (ESP) and Nitrile-specifier Protein (NSP) models refinement through 60 ns simulation of (**A**) ESP and (**B**) NSP backbone. RMSD is root mean square deviation.

Table 2 shows the binding affinity energies and affinity constants obtained for the protein-aglycone complexes at different pH. The stability of the docked complexes was analyzed based on affinity constants.

The interaction of NSP with aglycones derived from indolic glucosinolates resulted in an average binding affinity energy of −8.6 kcal/mol, showing no significant variations between ligands and

between the different pH. The affinity constants were found in the range of 1700–3300 (M) for these ligands. The interaction of NSP with aliphatic aglycones resulted in affinity binding energies between −6.7 and −5.8 kcal/mol with no apparent effect of pH. Binding affinity energy was lower for the interaction with indolic aglycones, and the affinity constant was lower for these ligands in comparison with aliphatic aglycones, indicating that indolic aglycones complexes are more stable.

The binding affinity energy of the complexes between ESP and aglycones derived from indolic glucosinolates was in average lower than those of aliphatic aglycones. The interaction between ESP and 4OHI3M was affected by pH showing no clear tendency. The other complexes were apparently not affected by pH in terms of binding affinity energy. Affinity constants varied between aglycones and pH, and were higher for the NSP complexes, in comparison with ESP. In turn, the ligand that showed the highest affinity constants was 4OHI3M, for both NSP and ESP.

The NSP–4OHI3M complex showed the highest affinity constant (kA) at pH 7 (3300 (M)). For ESP, the highest affinity constant was 2660 (M), at pH 7 complexed with I3M ligand, and K_A of the ESP–I3M complex remained constant at pH 1, pH 3, and pH 5 (220 (M)). For 4MSOB, the highest K_A was obtained at pH 5 for NSP and at pH 3 for ESP, giving values of 82 and 21 (M), respectively. The binding affinity energy was lower for the interaction of NSP with 4MSOB than for ESP with 4MSOB, at all pH. The lowest affinity constant was observed for the ESP-2PROP complex, being two orders of magnitude below the interaction between NSP–4OHI3M at pH 7.

Table 2. Binding affinity energy (kcal/mol) and affinity constant (k_A, M) obtained from the Autodock Vina program, for aglycone from five glucosinolates (GLS) (4OHI3M, I3M, 4MSOB, 3MSOP, and 2PROP), interacting with the nitrile-specifier protein (NSP) or epithiospecifier protein (ESP) at different pH value (1, 3, 5, 7), using iron (Fe^{2+}) as cofactor.

			Nitrile-Specifier Protein		**Epithiospecifier Protein**	
Precursor	**Aglycone**	**pH**	**Binding Affinity Energy (kcal/mol)**	**k_A (M)**	**Binding Affinity Energy (kcal/mol)**	**k_A (M)**
Hydroxy-glucobrassicin	4OHI3M	1	−8.7	2400	−7.0	140
		3	−8.6	2000	−5.7	15
		5	−8.5	1700	−6.8	96
		7	−8.9	3300	−5.9	21
Glucobrassicin	I3M	1	−8.5	1700	−7.3	220
		3	−8.6	2000	−7.3	220
		5	−8.6	2000	−7.3	220
		7	−8.5	1700	−7.4	270
Glucoraphanin	4MSOB	1	−6.5	58	−5.7	15
		3	−6.4	49	−5.9	21
		5	−6.7	82	−5.7	15
		7	−6.6	81	−5.6	13
Glucoiberin	3MSOP	1	−6.2	35	−5.2	6.5
		3	−6.2	35	−5.4	9.1
		5	−6.3	41	−5.5	11
		7	−6.3	41	−5.3	7.7
Sinigrin	2PROP	1	−6.0	25	−5.1	5.5
		3	−5.8	18	−5.2	6.5
		5	−5.8	18	−5.2	6.5
		7	−5.8	18	−5.0	4.6

The results suggest that the 4MSOB complexes are stabilized at acid pH, since the highest affinity constants for ESP–4MSOB and NSP–4MSOB were obtained at pH 3 and pH 5, respectively. The same order of magnitude of affinity constants may indicate that both ESP and NSP promote the formation of sulforaphane nitrile from glucoraphanin, at acid pH values (3; 5) in the presence of Fe^{2+}. These results

agree with those reported by Kissen et al. [23] and Backenköhler et al. [49], who found that the pH range of action for NSP and ESP from *A. thaliana* was pH 2–5.

Molecular docking simulations were conducted with the ligand that showed the highest affinity constants (4MSOB), and pH was set at pH 5 for NSP and at pH 3 for ESP. Fe^{2+} was included as a cofactor in all simulations. Figure 6 shows the interacting residues in the binding site of (A) NSP at pH 5, and (B) ESP at pH 3, with 4MSOB. Table 3 shows the atomic distances in the docked structures. The residues of NSP and ESP that interact directly with 4MSOB are at less than 6 (Å). Non-bonded interacting residues are summarized in Table 3.

Residues at the binding site of NSP were Arg220, Glu322, Ile168, Ser432, and Leu321. Among them, Fe^{2+} interacts with Glu322 forming an ionic interaction (Figure 6A). In addition, Fe^{2+} interacts with the oxygen of the carboxyl group of Leu321. Trp329 and His343 residues surround the binding site, stabilizing the aglycone (Table 3). The NSP residues that interact with the sulfonate group are Ile168, Arg220, and Ser432. This agrees with other studies that inform arginine is responsible for the stabilization of the sulfonate group in NSP [23,29,49].

Residues at the binding site of ESP were Val30, Arg80, Ser83, Ser135, Ile28, and Met81. The oxygen of the carboxyl group of Ile 28 and Met81 interact with Fe^{2+}. Simulations suggest that the Val30 amino group and the Ser83 side chain stabilize the sulfonate group (Figure 6B). However, a study of non-interacting residues located in the surrounding of the ESP binding site, showed that His322, Glu334, and Asp333 residues could interact with Fe^{2+}, forming a possible binding triad (Table 3), as reported by several authors [17,49].

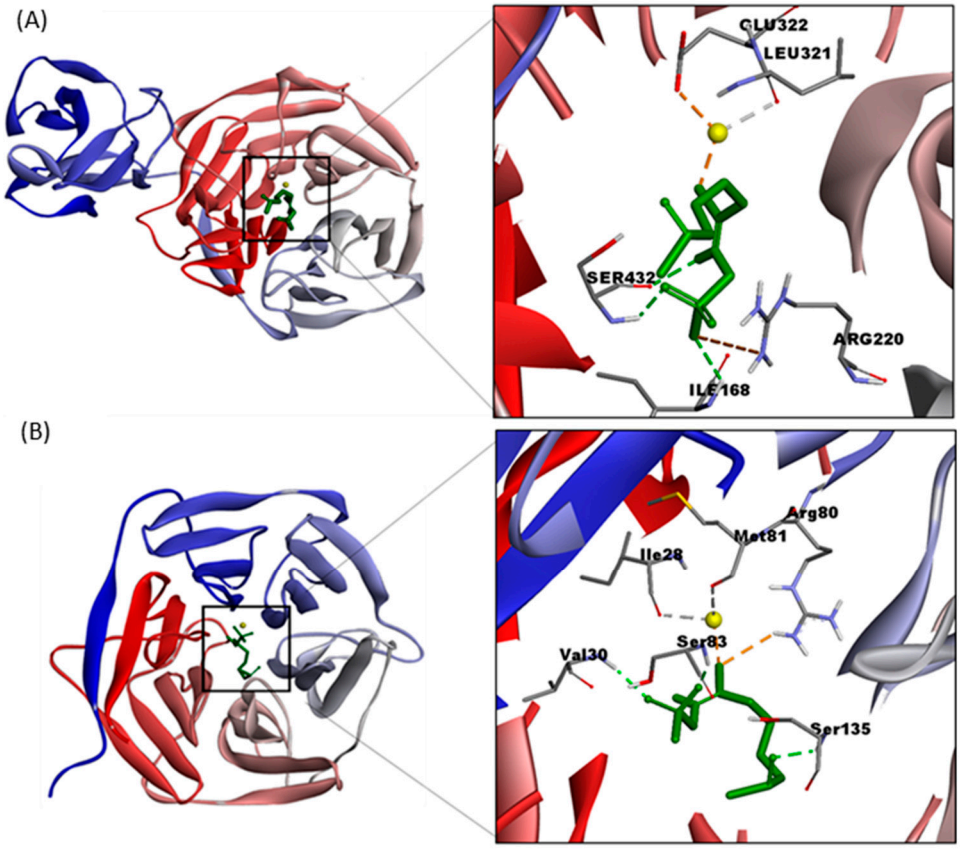

Figure 6. Three-dimensional structures of the complexes (**A**) NSP-4MSOB protonated at pH 5, and (**B**) ESP–4MSOB protonated at pH 3 and its interactions. In both complexes iron (Fe^{2+}) was added as a cofactor (showed in yellow color).

Brandt et al. [17] reported that in the case of ESP from *A. thaliana*, a Glu260 - Asp264 - His274 binding triad interacts with Fe^{+2} while Arg94 and Arg157 are suggested to stabilize the thiohydroxamate-

O-sulfonate group. Another study proposed that Gly186 and Val244 are responsible for the stabilization of aglycone in *A. thaliana* ESP [26]. In *A. thaliana* NSP (AtNSP3), iron-binding and NSP activity depend on Glu386, Asp390, and His394 [49]. Studies carried out on *Lepidium sativum* TFP (LsTFP), *A. thaliana* ESP (AtESP), and *Thlaspi arvense* TFP (TaTFP) showed that Arg94, Lis46, and Lis211 are involved in sulfate moiety binding [17].

The results obtained in this study suggest that broccoli ESP and NSP form more stable complexes with the aglycone 4MSOB at acid pH (3–5) in the presence of Fe^{+2}. These results are consistent with studies that indicate that the specifier proteins are iron-dependent and act at acid pH [6,17,24,50].

Table 3. Interactions of the complexes NSP-4MSOB at pH 5, and ESP-4MSOB at pH 3. Structural details of NSP-4MSOB and ESP-4MSOB complexes are given in Figure S6.

Complex	Number	Interaction	Distance (Å)	H-Donor	H-Acceptor
NSP-4MSOB pH5	1	ARG220	5.36	A:ARG220:NH1	:4MSOB:O13
	2	GLU322	2.47	:4MSOB:Fe5	A:GLU322:OE2
	3	ILE168	2.75	A:ILE168:H	:4MSOB:O13
	4	SER432	2.06	A:SER432:H	:4MSOB:O12
	5	SER432	2.40	:4MSOB:H8	A:SER432:O
	6	LEU321	2.57	:4MSOB:Fe5	A:LEU321:O
Non-bonded interacting residues	SER165, HIS166, ALA169, GLN170, GLY218, VAL219, MET221, VAL222, GLY320, TRP329, HIS343, SER430, ALA431, THR433, SER434				
ESP-4MSOB pH3	1	VAL30	2.11	A:VAL30:H	:4MSOB:O12
	2	ARG80	2.93	A:ARG80:HH21	:4MSOB:S14
	3	SER83	1.98	A:SER83:H	:4MSOB:O11
	4	SER135	2.12	A:SER135:H	:4MSOB:O2
	5	ILE28	2.54	:4MSOB:Fe3	A:ILE28:O
	6	MET81	2.50	:4MSOB:Fe3	A:MET81:O
Non-bonded interacting residues:	HIS26, GLY27, VAL31, GLY32, GLY78, THR79, GLY85, MET133, ALA134, ASP136, GLU137, HIS322, GLU334, ASP333.				

3. Materials and Methods

3.1. Plant Material

Broccoli (*Brassica oleracea* var. *italica*) heads (three days after harvesting) were purchased at the local market (Santiago, Chile) from a single supplier. Broccoli inflorescences were immediately processed for quantification of glucosinolates and their breakdown products.

3.2. Glucosinolates Identification

Identification of glucosinolates (GLS) was conducted by the method reported by Francisco et al. [38] through LC/UV-PAD/ESI-IT-MS^2. Fifty milligrams of broccoli inflorescences were extracted in 1.5 mL 70% methanol at 70 °C for 30 min with vortex mixing every 5 min. The samples were centrifuged (13,000× *g*, 15 min, 4 °C). The supernatants were collected, and methanol was completely removed using a rotary evaporator (Stuart RE-300, Chelmsford, United Kingdom) at 37 °C. The dry material obtained was dissolved in 1 mL ultrapure water and filtered through a 0.22 µm syringe PVDF filter (Millex Durapore®, Merck, Darmstadt, Germany). Separation of GSL was carried out in Agilent 1100 HPLC (Agilent Technologies Inc., Santa Clara, CA, USA) series equipped with a photodiode array detector (PAD) coupled to the ESI-IT Esquire 4000 electrospray-ion trap mass spectrometer (Bruker Daltonik GmbH, Karlsruhe, Germany). For the control of the HPLC system, the ChemStation for LC 3D program (Agilent Technologies Inc., Santa Clara, CA, USA) was used, and for the spectrometer control, the EsquireControl 5.2 program (Bruker Daltonik GmbH, Karlsruhe, Germany) was used. For

the HPLC separation, a Zorbax Eclipse Plus C18 column of 250 × 4.6 mm, 5 µm, and 100 Å (Agilent Technologies Inc., Santa Clara, CA, USA) was used. The separation of 20 µL of the sample was carried out at room temperature. The mobile phase consisted of the mixture of (A) 0.1% trifluoroacetic acid (TFA) and (B) acetonitrile/TFA (99.9: 0.1). A linear gradient was used starting with 0% of B in 0–5 min, reaching 17% of B in 15–17 min, 25% of B in 22 min, 35% B in 30 min, 50% B in 35 min, 99% of B in 50 min and in 55–65 min 0% of B. The flow rate was 1 mL/min. Absorbance at 227 nm was recorded. The analysis of chromatograms and mass spectra was performed through the program Data Analysis 3.2 (Bruker Daltonik GmbH, Karlsruhe, Germany). All measurements were performed in triplicate. The structures of the detected glucosinolates were confirmed according to their retention times and m/z signal (species $[M\text{-}H]^-$) (Table S2), MS/MS fragmentation as well as from the characteristic product ions (Table S3) [34–39,51–57]. The study of $MS^2[M-H]^-$ fragmentation of broccoli glucosinolates, shows specific product ions at m/z around 194, 242, 259, and 275, which correspond to the fragment ions from the aglycone side chain that have been reported by other authors [35,38,39].

3.3. Template Identification

The amino acid sequence of broccoli epithiospecifier protein (ESP) was obtained from UniProtKB protein sequence database (UniProtKB code: Q4TU02) [6]. To obtain the consensus amino acid sequence of broccoli nitrile specifier protein (NSP_BRO), the sequences Q9SDM9 (*A. thaliana*) [22], M4FIJ4 (*Brassica rapa subsp. pekinensis*) [58], A0A078G479 (*Brassica napus*) [59], and A0A0D3AD54 (*Brassica oleracea* var. *oleracea*) [60] were used as templates to perform multiple alignment.

3.4. ESP and NSP Modeling and Models Evaluation

Epithiospecifier protein ESP and nitrile-specifier protein (NSP) modeling was performed using the Iterative Threading ASSEmbly Refinement (I-TASSER) server 5.1 based on the ab initio/threading method [61,62]. I-TASSER uses a hierarchical protein structure modeling approach. A total of five three-dimensional (3D) models were generated for each protein (ESP and NSP); the model was selected based on the confidence score (C-Score), and validated by the evaluation tools ERRAT and Verify3D (available at http://services.mbi.ucla.edu).

3.5. Molecular Dynamics Simulation

Molecular dynamics simulations were carried out in GROMACS 5.0.7 [63–65]. The three-dimensional structure models of broccoli epithiospecifier protein (ESP) and nitrile-specifier protein (NSP) were selected based on highest C-score value (range of (−5.2)) and TM-score (higher than 0.5) given by Iterative Threading ASSEmbly Refinement (I-TASSER) [61,62,66] and were used for the MD simulation study with OPLS-AA/L all-atom force field (2001 amino acid dihedrals) [67]. An orthorhombic box with a predefined TIP3P water model was constructed around the 3D model. The box volume was minimized, and Fe^{2+} ions were added applying position restrains to the protein structure. The temperature and pressure of the system were kept constant at 298 K and 1.01325 bar after using the Berendsen weak-coupling method. A cut-off radius of 0.9 nm was used in the simulation of van der Waals and electrostatic interactions. Finally, a 60-ns production was carried out for ESP and NSP models using the particle mesh Ewald (PME) electrostatics method under NPT conditions. For analysis, final coordinates were saved every 20 ps, subjected to energy minimization. The refined model was used for molecular docking studies.

3.6. Molecular Docking

The binding affinities between epithiospecifier protein (ESP) and nitrile-specifier protein (NSP) and the aglycones derived from glucoraphanin (4MSOB-GLS), hydroxy-glucobrassicin (4OHI3M-GLS), glucobrassicin (I3M-GLS), glucoiberin (3MSOP-GLS), and sinigrin (2PROP-GLS) were obtained using AutoDock Vina 1.1.2 [68]. The aglycone structures were optimized by the LigPrep tool in Maestro of Schrödinger suite 1-2019 [69]. ESP and NSP models were pre-processed and prepared by Protein

Preparation Wizard in Maestro of Schrödinger suite 1-2019. Protonation and tautomeric states of each protein and ligand were adjusted at different pH (1, 3, 5, and 7), using the Epik 2.1 ionization tool of the Schrödinger suite 1-2019 [70,71]. Finally, the receptor grid was located at the binding sites of ESP and NSP. The identification of protein binding sites was made with the SiteMap tool of Schrödinger suite 1-2019 [46,47]. The grid was a cubic box, centered at the centroid of the binding site residues, that in case of the ESP center was: X: 54.995; Y: 58.009; Z: 63.829 and its size was: X: 96, Y: 96, Z: 96. The center of NSP was: X: 64.252, Y: 65.860, Z: 77.247, and its size was: X: 80, Y: 80, Z: 80. For protein-ligand docking, the exhaustiveness was 15. The most stable docking orientation was identified from the binding affinity score and hydrogen bond interaction to the binding site based on visual inspection. Discovery Studio 3.5 visualizer (DS 3.5) (DS, http://www.accelrys.com; Accelrys, Inc., San Diego, CA, USA) generated the 2D graphical visualization of ESP, NSP, and protein-ligand complexes.

4. Conclusions

Three-dimensional models of broccoli epithiospecifier protein (ESP) and nitrile-specifier protein (NSP) were constructed and deposited in Protein Models Database with the identifier PM0082617 and PM0082618, respectively. ESP model consisted of 29 β sheets and 29 loops, while the NSP model had 40 β sheets and 43 loops. Docking simulations showed that the NSP-4MSOB complex at pH 5 was more stable than ESP-4MSOB at pH3, in the presence of Fe^{2+}. The NSP residues that interact with 4MSOB and Fe^{2+} were Arg220, Glu322, Ile168, Ser432, and Leu321. Simulations showed that Fe^{2+} interacted with Glu322 and with Leu321. Ile168, Arg220, and Ser432 interact with sulfonate group. Trp329 and His343, located around the binding site, would be responsible for aglycone stabilization. The residues that belong to ESP binding site were Val30, Arg80, Ser83, Ser135, Ile28, and Met81. Docking simulations suggested that Fe^{2+} interacts with Ile 28 and Met81. Val30 and Ser83 interact with the sulfonate group, and His322 - Glu334 - Asp333 binding triad was proposed. The complexes containing 4MSOB were stabilized at pH = 3 for ESP and pH = 5 for NSP. Finally, pH determines the stability of the complexes, and the aglycone derived from glucoraphanin (4MSOB) has the highest affinity to both ESP and NSP. This agrees with the fact that glucoraphanin is the most abundant glucosinolate in broccoli florets. Our results will probably help in understanding the mechanism of action of specifier proteins and aglycones from broccoli.

Supplementary Materials: The following are available online at http://www.mdpi.com/1420-3049/25/4/772/s1, Figure S1: LC-MC spectra of (A) Glucoiberin, (B) Singrin, (C) Hidroxy-glucobrassicin and (D) Glucobrassicin; Figure S2: (A) NSP ERRAT validation model, (B) ESP ERRAT validation model; Figure S3: (A) NSP Verify 3D validation model, (B) ESP Verify 3D validation model; Figure S4: Hydrogen bonds number, obtained from 60-ns MD simulation for (A) ESP and (B) NSP models; Figure S5: Cluster size and RMS obtained from 60-ns MD simulation. (A) ESP cluster size, (B) NSP cluster size, (C) RMS for ESP and (D) RMS for NSP; Figure S6: Numbering of ligand atoms. (A) NSP-4MSOB pH 5 and (B) ESP-4MSOB pH 3, Table S1: Aminoacidic consensus sequence of NSP from broccoli homolog organisms (Q9SDM9, M4FIJ4, A0A078G479, and A0A0D3AD54); Table S2: Glucosinolates described in the literature; Table S3: m/z signals and characteristic fragments of glucosinolates.

Author Contributions: R.J. and G.D., performed the experiments, R.J. analyzed the results and contributed with discussion and writing the manuscript; M.A., contributed with discussion, writing the manuscript and funding, and I.M, contributed with experiments and writing the manuscript. All authors have read and agreed to the published version of the manuscript.

Funding: This research was funded by Vicerrectoría de Investigación, Desarrollo e Innovación through Proyecto POSTDOC_DICYT código 081911MO_POSTDOC, Universidad de Santiago de Chile.

Conflicts of Interest: The authors declare no conflict of interest.

References

1. Martinez-Ballesta, M.; Moreno, D.A.; Carvajal, M. The physiological importance of glucosinolates on plant response to abiotic stress in Brassica. *Int. J. Mol. Sci.* **2013**, *14*, 11607–11625. [CrossRef] [PubMed]
2. Agerbirk, N.; Olsen, C.E. Glucosinolate structures in evolution. *Phytochemistry* **2012**, *77*, 16–45. [CrossRef] [PubMed]

3. Bischoff, K.L. Chapter 40—Glucosinolates. In *Nutraceuticals*; Gupta, R.C., Ed.; Academic Press: Boston, MA, USA, 2016; pp. 551–554.
4. Hanschen, F.S.; Klopsch, R.; Oliviero, T.; Schreiner, M.; Verkerk, R.; Dekker, M. Optimizing isothiocyanate formation during enzymatic glucosinolate breakdown by adjusting pH value, temperature and dilution in Brassica vegetables and Arabidopsis thaliana. *Sci. Rep.* **2017**, *7*, 40807. [CrossRef] [PubMed]
5. Bell, L.; Wagstaff, C. Glucosinolates, Myrosinase Hydrolysis Products, and Flavonols Found in Rocket (Eruca sativa and Diplotaxis tenuifolia). *J. Agric. Food Chem.* **2014**, *62*, 4481–4492. [CrossRef]
6. Matusheski, N.V.; Swarup, R.; Juvik, J.A.; Mithen, R.; Bennett, M.; Jeffery, E.H. Epithiospecifier protein from broccoli (Brassica oleracea L. ssp italica) inhibits formation of the anticancer agent sulforaphane. *J. Agric. Food Chem.* **2006**, *54*, 2069–2076. [CrossRef]
7. Witzel, K.; Hanschen, F.S.; Schreiner, M.; Krumbein, A.; Ruppel, S.; Grosch, R. Verticillium suppression is associated with the glucosinolate composition of Arabidopsis thaliana leaves. *PLoS ONE* **2013**, *8*, e71877. [CrossRef]
8. Jorgensen, M.E.; Nour-Eldin, H.H.; Halkier, B.A. Transport of defense compounds from source to sink: Lessons learned from glucosinolates. *Trends Plant Sci.* **2015**, *20*, 508–514. [CrossRef]
9. Koroleva, O.A.; Gibson, T.M.; Cramer, R.; Stain, C. Glucosinolate-accumulating S-cells in Arabidopsis leaves and flower stalks undergo programmed cell death at early stages of differentiation. *Plant J.* **2010**, *64*, 456–469. [CrossRef]
10. Wittstock, U.; Burow, M. Glucosinolate breakdown in Arabidopsis: Mechanism, regulation and biological significance. *Arab. Book* **2010**, *8*, e0134. [CrossRef]
11. Kissen, R.; Rossiter, J.T.; Bones, A.M.J.P.R. The 'mustard oil bomb': Not so easy to assemble?! Localization, expression and distribution of the components of the myrosinase enzyme system. *Phytochem. Rev.* **2009**, *8*, 69–86. [CrossRef]
12. Latte, K.P.; Appel, K.E.; Lampen, A. Health benefits and possible risks of broccoli—An overview. *Food Chem. Toxicol.* **2011**, *49*, 3287–3309. [CrossRef] [PubMed]
13. Burow, M.; Markert, J.; Gershenzon, J.; Wittstock, U. Comparative biochemical characterization of nitrile-forming proteins from plants and insects that alter myrosinase-catalysed hydrolysis of glucosinolates. *FEBS J.* **2006**, *273*, 2432–2446. [CrossRef] [PubMed]
14. Tookey, H.L. Crambe thioglucoside glucohydrolase (EC 3.2.3.1): Separation of a protein required for epithiobutane formation. *Can. J. Biochem.* **1973**, *51*, 1654–1660. [CrossRef] [PubMed]
15. Wittstock, U.; Burow, M. Tipping the scales–specifier proteins in glucosinolate hydrolysis. *IUBMB Life* **2007**, *59*, 744–751. [CrossRef]
16. Foo, H.L.; Grønning, L.M.; Goodenough, L.; Bones, A.M.; Danielsen, B.E.; Whiting, D.A.; Rossiter, J.T. Purification and characterisation of epithiospecifier protein from Brassica napus: Enzymic intramolecular sulphur addition within alkenyl thiohydroximates derived from alkenyl glucosinolate hydrolysis. *FEBS Lett.* **2000**, *468*, 243–246. [CrossRef]
17. Brandt, W.; Backenköhler, A.; Schulze, E.; Plock, A.; Herberg, T.; Roese, E.; Wittstock, U. Molecular models and mutational analyses of plant specifier proteins suggest active site residues and reaction mechanism. *Plant Mol. Biol.* **2014**, *84*, 173–188. [CrossRef]
18. Walker, N.J.; Gray, I.K. Glucosinolate of land cress (Coronopus didymus) and its enzymic degradation products as precursors of off-flavor in milk—A review. *J. Agric. Food Chem.* **1970**, *18*, 346–352. [CrossRef]
19. Schlüter, M.; Gmelin, R. Abnormale enzymatische spaltung von 4-methylthiobutylglucosinolat in frischpflanzen von Eruca sativa. *Phytochemistry* **1972**, *11*, 3427–3431. [CrossRef]
20. Burow, M.; Bergner, A.; Gershenzon, J.; Wittstock, U. Glucosinolate hydrolysis in Lepidium sativum–identification of the thiocyanate-forming protein. *Plant Mol. Biol.* **2007**, *63*, 49–61. [CrossRef]
21. Kuchernig, J.C.; Backenköhler, A.; Lübbecke, M.; Burow, M.; Wittstock, U. A thiocyanate-forming protein generates multiple products upon allylglucosinolate breakdown in Thlaspi arvense. *Phytochemistry* **2011**, *72*, 1699–1709. [CrossRef]
22. Burow, M.; Losansky, A.; Müller, R.; Plock, A.; Kliebenstein, D.J.; Wittstock, U. The Genetic Basis of Constitutive and Herbivore-Induced ESP-Independent Nitrile Formation in Arabidopsis. *Plant Physiol.* **2009**, *149*, 561–574. [CrossRef] [PubMed]
23. Kissen, R.; Bones, A.M. Nitrile-specifier proteins involved in glucosinolate hydrolysis in Arabidopsis thaliana. *J. Biol. Chem.* **2009**, *284*, 12057–12070. [CrossRef] [PubMed]

24. Kong, X.Y.; Kissen, R.; Bones, A.M. Characterization of recombinant nitrile-specifier proteins (NSPs) of Arabidopsis thaliana: Dependency on Fe(II) ions and the effect of glucosinolate substrate and reaction conditions. *Phytochemistry* **2012**, *84*, 7–17. [CrossRef] [PubMed]
25. Bernardi, R.; Negri, A.; Ronchi, S.; Palmieri, S. Isolation of the epithiospecifier protein from oil-rape (Brassica napus ssp. oleifera) seed and its characterization. *FEBS Lett.* **2000**, *467*, 296–298. [CrossRef]
26. Zhang, W.; Wang, W.; Liu, Z.; Xie, Y.; Wang, H.; Mu, Y.; Huang, Y.; Feng, Y. Crystal structure of the Epithiospecifier Protein, ESP from Arabidopsis thaliana provides insights into its product specificity. *Biochem. Biophys. Res. Commun.* **2016**, *478*, 746–751. [CrossRef] [PubMed]
27. Wittstock, U.; Agerbirk, N.; Stauber, E.J.; Olsen, C.E.; Hippler, M.; Mitchell-Olds, T.; Gershenzon, J.; Vogel, H. Successful herbivore attack due to metabolic diversion of a plant chemical defense. *Proc. Natl. Acad. Sci. USA* **2004**, *101*, 4859–4864. [CrossRef]
28. Kuchernig, J.C.; Burow, M.; Wittstock, U. Evolution of specifier proteins in glucosinolate-containing plants. *BMC Evol. Biol.* **2012**, *12*, 127. [CrossRef]
29. Zhang, W.; Zhou, Y.; Wang, K.; Dong, Y.; Wang, W.; Feng, Y. Crystal structure of the nitrile-specifier protein NSP1 from Arabidopsis thaliana. *Biochem. Biophys. Res. Commun.* **2017**, *488*, 147–152. [CrossRef]
30. Matusheski, N.V.; Juvik, J.A.; Jeffery, E.H. Heating decreases epithiospecifier protein activity and increases sulforaphane formation in broccoli. *Phytochemistry* **2004**, *65*, 1273–1281. [CrossRef]
31. Perez, C.; Barrientos, H.; Román, J.; Mahn, A. Optimization of a blanching step to maximize sulforaphane synthesis in broccoli florets. *Food Chem.* **2014**, *145*, 264–271. [CrossRef]
32. Westphal, A.; Riedl, K.M.; Cooperstone, J.L.; Kamat, S.; Balasubramaniam, V.M.; Schwartz, S.J.; Böhm, V. High-Pressure Processing of Broccoli Sprouts: Influence on Bioactivation of Glucosinolates to Isothiocyanates. *J. Agric. Food Chem.* **2017**, *65*, 8578–8585. [CrossRef]
33. Tabart, J.; Pincemail, J.; Kevers, C.; Defraigne, J.O.; Dommes, J. Processing effects on antioxidant, glucosinolate, and sulforaphane contents in broccoli and red cabbage. *Eur. Food Res. Technol.* **2018**, *244*, 2085–2094. [CrossRef]
34. Lee, K.C.; Chan, W.; Liang, Z.; Liu, N.; Zhao, Z.; Lee, A.W.M.; Cai, Z. Rapid screening method for intact glucosinolates in Chinese medicinal herbs by using liquid chromatography coupled with electrospray ionization ion trap mass spectrometry in negative ion mode. *Rapid Commun. Mass Spectrom.* **2008**, *22*, 2825–2834. [CrossRef] [PubMed]
35. Rochfort, S.J.; Trenerry, V.C.; Imsic, M.; Panozzo, J.; Jones, R. Class targeted metabolomics: ESI ion trap screening methods for glucosinolates based on MSn fragmentation. *Phytochemistry* **2008**, *69*, 1671–1679. [CrossRef] [PubMed]
36. Velasco, P.; Francisco, M.; Moreno, D.A.; Ferreres, F.; García-Viguera, C.; Cartea, M.E. Phytochemical fingerprinting of vegetable Brassica oleracea and Brassica napus by simultaneous identification of glucosinolates and phenolics. *Phytochem. Anal.* **2011**, *22*, 144–152. [CrossRef] [PubMed]
37. Cataldi, T.R.I.; Rubino, A.; Lelario, F.; Bufo, S.A. Naturally occurring glucosinolates in plant extracts of rocket salad (Eruca sativa L.) identified by liquid chromatography coupled with negative ion electrospray ionization and quadrupole ion-trap mass spectrometry. *Rapid Commun. Mass Spectrom.* **2007**, *21*, 2374–2388. [CrossRef] [PubMed]
38. Francisco, M.; Moreno, D.A.; Cartea, M.E.; Ferreres, F.; García-Viguera, C.; Velasco, P. Simultaneous identification of glucosinolates and phenolic compounds in a representative collection of vegetable Brassica rapa. *J. Chromatogr. A* **2009**, *1216*, 6611–6619. [CrossRef]
39. Fabre, N.; Poinsot, V.; Debrauwer, L.; Vigor, C.; Tulliez, J.; Fourasté, I.; Moulis, C. Characterisation of glucosinolates using electrospray ion trap and electrospray quadrupole time-of-flight mass spectrometry. *Phytochem. Anal.* **2007**, *18*, 306–319. [CrossRef]
40. Leng, C.Q.; Zhang, Y.; Wang, M.; Wang, P.; Gu, Z.; Yang, R. Dynamic variation of glucosinolates and isothiocyanates in broccoli sprouts during hydrolysis. *Sci. Hortic.* **2019**, *255*, 128–133. [CrossRef]
41. Wang, J.S.; Yu, H.; Zhao, Z.; Sheng, X.; Shen, Y.; Gu, H. Natural Variation of Glucosinolates and Their Breakdown Products in Broccoli (Brassica oleracea var. italica) Seeds. *J. Agric. Food Chem.* **2019**, *67*, 12528–12537. [CrossRef]
42. Schonhof, I.; Krumbein, A.; Bruckner, B. Genotypic effects on glucosinolates and sensory properties of broccoli and cauliflower. *Nahrung* **2004**, *48*, 25–33. [CrossRef]
43. Steinbrecher, A.; Linseisen, J. Dietary intake of individual glucosinolates in participants of the EPIC-Heidelberg cohort study. *Ann. Nutr. Metab.* **2009**, *54*, 87–96. [CrossRef]

44. Colovos, C.; Yeates, T.O. Verification of protein structures: Patterns of nonbonded atomic interactions. *Protein Sci.* **1993**, *2*, 1511–1519. [CrossRef]
45. Eisenberg, D.; Luthy, R.; Bowie, J.U. VERIFY3D: Assessment of protein models with three-dimensional profiles. *Methods Enzymol.* **1997**, *277*, 396–404.
46. Halgren, T.A. Identifying and Characterizing Binding Sites and Assessing Druggability. *J. Chem. Inf. Modeling* **2009**, *49*, 377–389. [CrossRef] [PubMed]
47. Halgren, T. New method for fast and accurate binding-site identification and analysis. *Chem. Biol. Drug Des.* **2007**, *69*, 146–148. [CrossRef] [PubMed]
48. Nayal, M.; Honig, B. On the nature of cavities on protein surfaces: Application to the identification of drug-binding sites. *Proteins* **2006**, *63*, 892–906. [CrossRef] [PubMed]
49. Backenköhler, A.; Eisenschmidt, D.; Schneegans, N.; Strieker, M.; Brandt, W.; Wittstock, U. Iron is a centrally bound cofactor of specifier proteins involved in glucosinolate breakdown. *PLoS ONE* **2018**, *13*, e0205755. [CrossRef]
50. Barba, F.J.; Nikmaram, N.; Roohinejad, S.; Khelfa, A.; Zhu, Z.; Koubaa, M. Bioavailability of Glucosinolates and Their Breakdown Products: Impact of Processing. *Front. Nutr.* **2016**, *3*, 24. [CrossRef]
51. Lee, K.C.; Cheuk, M.W.; Chan, W.; Lee, A.W.M.; Zhao, Z.Z.; Jiang, Z.H.; Cai, Z. Determination of glucosinolates in traditional Chinese herbs by high-performance liquid chromatography and electrospray ionization mass spectrometry. *Anal. Bioanal. Chem.* **2006**, *386*, 2225–2232. [CrossRef]
52. Millán, S.; Sampedro, M.C.; Gallejones, P.; Castellón, A.; Ibargoitia, M.L.; Goicolea, M.A.; Barrio, R.J. Identification and quantification of glucosinolates in rapeseed using liquid chromatography–ion trap mass spectrometry. *Anal. Bioanal. Chem.* **2009**, *394*, 1661–1669. [CrossRef] [PubMed]
53. Cataldi, T.R.; Lelario, F.; Orlando, D.; Bufo, S.A. Collision-induced dissociation of the A + 2 isotope ion facilitates glucosinolates structure elucidation by electrospray ionization-tandem mass spectrometry with a linear quadrupole ion trap. *Anal. Chem.* **2010**, *82*, 5686–5696. [CrossRef] [PubMed]
54. Ediage, E.N.; Di Mavungu, J.D.; Scippo, M.L.; Schneider, Y.J.; Larondelle, Y.; Callebaut, A.; Robbens, J.; Van Peteghem, C.; De Saeger, S. Screening, identification and quantification of glucosinolates in black radish (Raphanus sativus L. niger) based dietary supplements using liquid chromatography coupled with a photodiode array and liquid chromatography-mass spectrometry. *J. Chromatogr. A* **2011**, *1218*, 4395–4405. [CrossRef]
55. Lelario, F.; Bianco, G.; Bufo, S.A.; Cataldi, T.R. Establishing the occurrence of major and minor glucosinolates in Brassicaceae by LC-ESI-hybrid linear ion-trap and Fourier-transform ion cyclotron resonance mass spectrometry. *Phytochemistry* **2012**, *73*, 74–83. [CrossRef] [PubMed]
56. Bianco, G.; Lelario, F.; Battista, F.G.; Bufo, S.A.; Cataldi, T.R. Identification of glucosinolates in capers by LC-ESI-hybrid linear ion trap with Fourier transform ion cyclotron resonance mass spectrometry (LC-ESI-LTQ-FTICR MS) and infrared multiphoton dissociation. *J. Mass Spectrom.* **2012**, *47*, 1160–1169. [CrossRef] [PubMed]
57. Martínez-Hernández, G.B.; Artés-Hernández, F.; Gómez, P.A.; Artés, F. Induced changes in bioactive compounds of kailan-hybrid broccoli after innovative processing and storage. *J. Funct. Foods* **2013**, *5*, 133–143. [CrossRef]
58. Wang, X.; Wang, H.; Wang, J.; Sun, R.; Wu, J.; Liu, S.; Bai, Y.; Mun, J.H.; Bancroft, I.; Cheng, F.; et al. The genome of the mesopolyploid crop species Brassica rapa. *Nat. Genet.* **2011**, *43*, 1035–1039. [CrossRef]
59. Chalhoub, B.; Denoeud, F.; Liu, S.; Parkin, I.A.; Tang, H.; Wang, X.; Chiquet, J.; Belcram, H.; Tong, C.; Samans, B.; et al. Early allopolyploid evolution in the post-Neolithic Brassica napus oilseed genome. *Science* **2014**, *345*, 950–953. [CrossRef]
60. Parkin, I.A.P.; Koh, C.; Tang, H.; Robinson, S.J.; Kagale, S.; Clarke, W.E.; Town, C.D.; Nixon, J.; Krishnakumar, V.; Bidwell, S.L.; et al. Transcriptome and methylome profiling reveals relics of genome dominance in the mesopolyploid Brassica oleracea. *Genome Biol.* **2014**, *15*, R77. [CrossRef]
61. Roy, A.; Kucukural, A.; Zhang, Y. I-TASSER: A unified platform for automated protein structure and function prediction. *Nat. Protoc.* **2010**, *5*, 725–738. [CrossRef]
62. Zhang, Y. I-TASSER server for protein 3D structure prediction. *BMC Bioinform.* **2008**, *9*, 40. [CrossRef] [PubMed]
63. Berendsen, H.J.C.; van der Spoel, D.; van Drunen, R. GROMACS: A message-passing parallel molecular dynamics implementation. *Comput. Phys. Commun.* **1995**, *91*, 43–56. [CrossRef]

64. Hess, B.; Kutzner, C.; Van Der Spoel, D.; Lindahl, E. GROMACS 4: Algorithms for Highly Efficient, Load-Balanced, and Scalable Molecular Simulation. *J. Chem. Theory Comput.* **2008**, *4*, 435–447. [CrossRef] [PubMed]
65. Lee, J.; Cheng, X.; Swails, J.M.; Yeom, M.S.; Eastman, P.K.; Lemkul, J.A.; Wei, S.; Buckner, J.; Jeong, J.C.; Qi, Y.; et al. CHARMM-GUI Input Generator for NAMD, GROMACS, AMBER, OpenMM, and CHARMM/OpenMM Simulations Using the CHARMM36 Additive Force Field. *J. Chem. Theory Comput.* **2016**, *12*, 405–413. [CrossRef]
66. Yang, J.; Yan, R.; Roy, A.; Xu, D.; Poisson, J.; Zhang, Y. The I-TASSER Suite: Protein structure and function prediction. *Nat. Methods* **2015**, *12*, 7–8. [CrossRef]
67. Kaminski, G.A.; Friesner, R.A.; Tirado-Rives, J.; Jorgensen, W.L. Evaluation and Reparametrization of the OPLS-AA Force Field for Proteins via Comparison with Accurate Quantum Chemical Calculations on Peptides. *J. Phys. Chem. B* **2001**, *105*, 6474–6487. [CrossRef]
68. Trott, O.; Olson, A.J. AutoDock Vina: Improving the speed and accuracy of docking with a new scoring function, efficient optimization, and multithreading. *J. Comput. Chem.* **2010**, *31*, 455–461. [CrossRef]
69. *Schrödinger Release 2016-3: LigPrep*; Schrödinger, LLC: New York, NY, USA, 2016.
70. Epik, S. (Ed.) *Schrödinger Release 2018-1: Schrödinger Suite 2018-1 Protein Preparation Wizard*; LLC: New York, NY, USA, 2016; Impact, Schrödinger, LLC: New York, NY, USA, 2016; Prime, Schrödinger, LLC: New York, NY, USA, 2018.
71. Sastry, G.M.; Adzhigirey, M.; Day, T.; Annabhimoju, R.; Sherman, W. Protein and ligand preparation: Parameters, protocols, and influence on virtual screening enrichments. *J. Comput. Aid. Mol. Des.* **2013**, *27*, 221–234. [CrossRef]

Sample Availability: Samples of the compounds are available from the authors.